This article was downloaded by: [Stanford University]
On: 16 August 2013, At: 16:19
Publisher: Taylor & Francis
Informa Ltd Registered in England and Wales Registered Number: 1072954 Registered office: Mortimer House, 37-41 Mortimer Street, London W1T 3JH, UK

Journal of Modern Optics
Publication details, including instructions for authors and subscription information:
http://www.tandfonline.com/loi/tmop20

Electromagnetic forces in the vacuum region of laser-driven layered grating structures

T. Plettner [a], R.L. Byer [a] & B. Montazeri [a]
[a] Department of Applied Physics, Stanford University, Stanford, CA 94305, USA
Published online: 01 Sep 2011.

To cite this article: T. Plettner , R.L. Byer & B. Montazeri (2011) Electromagnetic forces in the vacuum region of laser-driven layered grating structures, Journal of Modern Optics, 58:17, 1518-1528, DOI: 10.1080/09500340.2011.611914

To link to this article: http://dx.doi.org/10.1080/09500340.2011.611914

PLEASE SCROLL DOWN FOR ARTICLE

Taylor & Francis makes every effort to ensure the accuracy of all the information (the "Content") contained in the publications on our platform. However, Taylor & Francis, our agents, and our licensors make no representations or warranties whatsoever as to the accuracy, completeness, or suitability for any purpose of the Content. Any opinions and views expressed in this publication are the opinions and views of the authors, and are not the views of or endorsed by Taylor & Francis. The accuracy of the Content should not be relied upon and should be independently verified with primary sources of information. Taylor and Francis shall not be liable for any losses, actions, claims, proceedings, demands, costs, expenses, damages, and other liabilities whatsoever or howsoever caused arising directly or indirectly in connection with, in relation to or arising out of the use of the Content.

This article may be used for research, teaching, and private study purposes. Any substantial or systematic reproduction, redistribution, reselling, loan, sub-licensing, systematic supply, or distribution in any form to anyone is expressly forbidden. Terms & Conditions of access and use can be found at http://www.tandfonline.com/page/terms-and-conditions

Journal of Modern Optics
Vol. 58, No. 17, 10 October 2011, 1518–1528

Taylor & Francis
Taylor & Francis Group

Electromagnetic forces in the vacuum region of laser-driven layered grating structures

T. Plettner*, R.L. Byer and B. Montazeri

Department of Applied Physics, Stanford University, Stanford, CA 94305, USA

(*Received 15 May 2011; final version received 20 July 2011*)

Symmetric multilayer grating structures that have an embedded vacuum channel and that are powered by external laser beams are analyzed for their ability to manipulate charged particle beams. It is shown that acceleration, deflection and focusing forces can all be generated in a controlled fashion from the same grating architecture and by adjustment of phase of the incoming laser beams

Keywords: multilayer grating; grating eigenmode; electromagnetic force

Downloaded by [Stanford University] at 16:19 16 August 2013

1. Introduction

Photonic devices such as gratings [1–3] or photonic bandgap structures [4–6] designed for the manipulation of charged particles are capturing ever-increasing attention, in particular for the application of laser-driven particle acceleration. However, besides acceleration of high-energy particles, little attention has been devoted to their application for deflection or to manipulate low-energy charged particles. This paper expands on previous work on laser-driven deflection from gratings [7] and presents a comprehensive analysis of dielectric grating structures devoted to accelerate, deflect or to focus both low-velocity ($v \sim 0.2$–$0.99c$) and near-speed of light ($v > 0.99c$) charged particles.

The operation of grating structures for charged particle manipulation described in this paper is as follows: a free-space external laser beam generates a series of grating diffraction modes inside a vacuum channel of the multilayer grating structure that is provided for the particle beam. The design is chosen such that one of these diffraction modes possesses a phase velocity that matches that of the particle beam, which from here on is referred to as the synchronous mode. The eigenmode corresponding to the first space harmonic usually has the largest amplitude. Without any loss of generality it will be assumed that the grating period is chosen such that the first space harmonic is phase synchronous with the speed of the particle. The deflection, acceleration or deceleration force that results from the phase-synchronous space harmonic mode depends on its electric and magnetic field components and is determined by application of Lorentz' force.

We employ an eigenmode decomposition method developed by Pai and Awada [8] to evaluate the electromagnetic fields and their space harmonics inside multilayer grating structures. The main advantage of this method over direct spatial field numerical approaches lies in its ability to directly evaluate the spectrum of space harmonics, and more importantly, the particular mode that is phase-synchronous with the particle and that is responsible its cumulative interaction. This mode can be either an evanescent or a longitudinal wave. The original formulation by Pai and Awada does not include a treatment of longitudinal-wave eigenmodes nor of the TM polarization.

This paper is organized as follows: Section 2 presents an overview of the grating eigenmode decomposition method and Section 3 describes the expansion of the model to include longitudinal-wave eigenmodes. Section 4 describes the boundary condition for the TM polarization. Section 5 describes a traditional open grating geometry and its shortcomings and Section 6 describes a symmetric closed vacuum channel grating configuration that is capable of generating acceleration, deflection and focusing forces by adjustment of the grating orientation and laser beam phase.

2. Overview of the eigenmode decomposition method

The grating structure is modeled as a stack of discrete layers of dielectric material, as shown in Figure 1(*a*). Within each layer the dielectric is assumed to remain uniform along the y and z coordinates, but can vary along the x-axis with a periodicity equal to that of the grating and its space harmonics. The structure is invariant along the z-direction and the region of

*Corresponding author. Email: tomas.plettner@gmail.com

ISSN 0950–0340 print/ISSN 1362–3044 online
© 2011 Taylor & Francis
http://dx.doi.org/10.1080/09500340.2011.611914
http://www.tandfonline.com

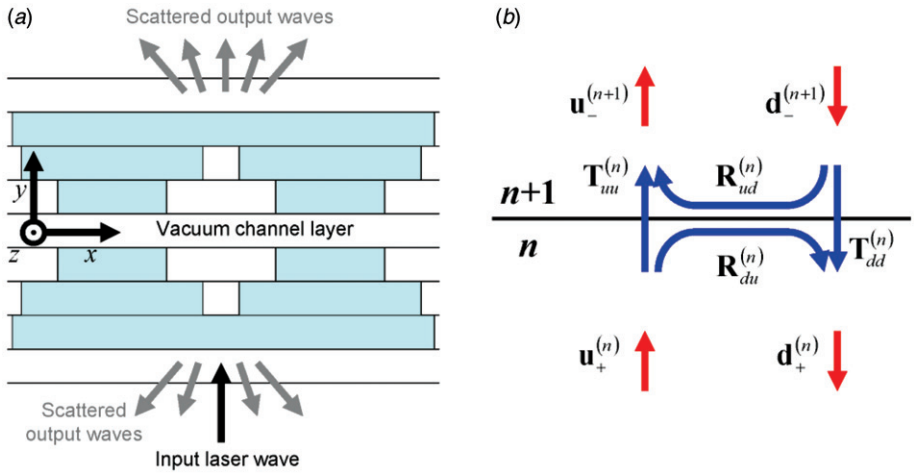

Figure 1. (*a*) Top-view schematic of a conceptual multi-layer grating accelerator structure. (*b*) Diagram of the up and down modes at the interface between layer n and layer $n+1$, and the definition of the transmission and reflection coefficients. (The color version of this figure is included in the online version of the journal.)

Downloaded by [Stanford University] at 16:19 16 August 2013

interest is assumed to have no net charge density. The incident electromagnetic wave is also invariant along the z-direction and hence the field solution is two-dimensional and possesses independent TE and TM polarizations. Both polarization modes are fully characterized by the field component aligned with the z-direction. The particle beam is assumed to travel inside the vacuum channel layer within the xz-plane.

The grating structures that are of interest in this paper are symmetric and include a vacuum layer which serves as the transport channel for the electron beam. The objective is to determine the space harmonics of the electromagnetic field inside this layer. Consider the nth layer of the grating. For the TM polarization the magnetic field is parallel to the z-direction in Figure 1(*a*) and is governed by Helmholz' equation

$$\left(\frac{\mathrm{d}^2}{\mathrm{d}x^2}+\frac{\mathrm{d}^2}{\mathrm{d}y^2}+\omega^2\mu\varepsilon^{(n)}(x)\right)B_z(x,y)=0, \tag{1}$$

where $\varepsilon^{(n)}(x)$ is the dielectric function of the nth layer and satisfies $\varepsilon^{(n)}(x)=\varepsilon^{(n)}(x+\lambda_p)$ and λ_p is the period of the grating. The periodicity in x allows for application of Floquet's theorem (see, for example, [9]) where the field is described by a superposition of space harmonics:

$$B_z^{(n)}(x,y)=\sum_{m=-\infty}^{+\infty}\psi_m^{(n)}(y)e^{i(mk_p+k_0)x}, \tag{2}$$

where k_p is the grating k-vector $k_p=2\pi/\lambda_p$. The superscript in Equation (2) refers to the layer number and the subscript denotes the mode number. The objective is to determine the amplitude of the space harmonic modes $\psi_m^{(n)}(y)$ within each layer of the grating structure. A Fourier transformation of Equation (1) yields the matrix equation

$$\left(\frac{\mathrm{d}^2}{\mathrm{d}y^2}+\mathbf{K}+\mathbf{S}^{(n)}\right)\mathbf{\Psi}^{(n)}=0. \tag{3}$$

The matrices $\mathbf{K}$ and $\mathbf{S}^{(n)}$ have the same meaning as in the formulation presented by Pai and Awada. Next, a linear transformation is applied to diagonalize Equation (3) and to obtain the following matrix equation

$$\left(\frac{\mathrm{d}^2}{\mathrm{d}y^2}+\mathbf{E}^2(n)\right)\mathbf{\Phi}^{(n)}=0 \tag{4}$$

where $\mathbf{\Phi}^{(n)}$ represents the spectrum of grating layer eigenmodes, which are either propagating or evanescent depending on the value of the corresponding entry in the eigenvalue diagonal matrix $\mathbf{E}^2(n)$. Each grating layer possesses a unique eigenmode equation and the set of eigenmodes in each layer is related to the corresponding space harmonics by the following matrix transformation:

$$\mathbf{\Phi}^{(n)}=\mathbf{M}^{(n)}\mathbf{\Psi}^{(n)}, \tag{5}$$

where $\mathbf{M}^{(n)}$ is the transformation matrix that diagonalizes Equation (3). If the layer in question is a uniform medium, like the vacuum channel layer, there exists a transformation where grating eigenmodes are equal to the space harmonics; $\mathbf{\Phi}^{(n)}=\mathbf{\Psi}^{(n)}$. The possibility of a longitudinal wave, not analyzed in the original formulation, occurs when the eigenvalue is zero. The consequences for the inclusion of these modes are described in Section 3.

Downloaded by [Stanford University] at 16:19 16 August 2013

3. Addition of longitudinal wave eigenmodes

Consider a particular mode j having an eigenvalue equal to zero. Such a mode can occur when the laser wavelength matches the grating period. For this mode Equation (4) reduces to

$$\left(\frac{\mathrm{d}^2}{\mathrm{d}y^2} + 0\right)\mathbf{\Phi}_j^{(n)} = 0. \tag{6}$$

The general solution to this differential equation is $\mathbf{\Phi}_j^{(n)} = C_1 + C_2 y$, where the formulation by Pai and Awada does not consider the possibility of the linear dependence on y for this type of eigenmode. Nonetheless, in the same fashion as performed by Pai and Awada the solution can be expressed as a linear superposition of upward-propagating modes, $U_j^{(n)}$, and downward propagating modes, $D_j^{(n)}$, that are defined as

$$\begin{aligned} U_j^{(n)} &= 1 - \kappa^{(n)} y, \\ D_j^{(n)} &= 1 + \kappa^{(n)} y. \end{aligned} \tag{7}$$

These modes are both solutions to Equation (6), and their linear superposition describes the speed-of-light mode that propagates in the layer n. If the layer n is vacuum, $U_j^{(n)}$ and $D_j^{(n)}$ are longitudinal waves with speed-of-light phase velocity. This is the mode of interest for acceleration of relativistic particles. For the TM polarization the magnetic field of the mode $U_j^{(n)}$ is described by

$$\begin{aligned} &B_x(x, y; t) = 0, \quad B_y(x, y; t) = 0, \\ &B_z(x, y; t) = A\left(1 - \kappa^{(n)} y\right) e^{ikx - i\omega t}. \end{aligned} \tag{8}$$

With $\vec{\nabla} \times \vec{B} = -\mu\varepsilon i\omega \vec{E}$ it can be shown that inside a vacuum layer the longitudinal electric field component, $E_x(x, y; t)$, is nonzero and constant along the y-direction. The other field components grow linearly with y, and therefore in the absence of boundaries at finite values of y the amplitude A in Equation (8) has to be zero.

4. Boundary conditions for the TM polarization

Consider the interface between grating layers n and $n+1$, as is shown in Figure 1(*b*). For the TE polarization the boundary condition between grating layers simplifies to a continuity of the field amplitude and its first derivative across the layer boundary. The plane wave eigenmodes are grouped into a set of up (**u**) and down (**d**) propagating modes that are connected from one layer to the next by a 2×2 transmission matrix. For the TM polarization the boundary conditions are

$$\begin{aligned} B_z\left(y_+^{(n)}\right) &= B_z\left(y_-^{(n+1)}\right), \\ E_x\left(y_+^{(n)}\right) &= E_x\left(y_-^{(n+1)}\right). \end{aligned} \tag{9}$$

The plus subscript refers to the top of the nth layer and the minus sign refers to the bottom of the $(n+1)$th layer. These field components are to be expressed in terms of the layer eigenmode components. The first boundary condition of Equation (9) reads $\mathbf{\Psi}^{(n)} = \mathbf{\Psi}^{(n+1)}$ for the space harmonics, which means that by Equation (5) the layer eigenmodes have to satisfy

$$\left(\mathbf{M}^{(n)}\right)^{-1} \mathbf{\Phi}^{(n)} = \left(\mathbf{M}^{(n+1)}\right)^{-1} \mathbf{\Phi}^{(n+1)}. \tag{10}$$

For the second boundary condition the electric field is to be expressed in terms of the layer eigenmodes that describe the B_z field. After some algebra one can show that the second boundary condition results in

$$\left(\mathbf{S}^{(n)}\right)^{-1} \left(\mathbf{M}^{(n)}\right)^{-1} d_y \mathbf{\Phi}^{(n)} = \left(\mathbf{S}^{(n+1)}\right)^{-1} \left(\mathbf{M}^{(n+1)}\right)^{-1} d_y \mathbf{\Phi}^{(n+1)}, \tag{11}$$

where d_y is the derivative with respect to the y coordinate. $\mathbf{\Phi}^{(n)}$ represents the spectrum of up- and downward propagating eigenmodes of the nth grating layer. The solution for the eigenmode boundary conditions of Equations (10) and (11) is presented in Appendix 1.

5. Open grating structures

Metallic open-grating structures have been studied extensively for particle acceleration [10,11] or for generation of radiation [12,13]. Although they are not the main object in this paper they do represent the simplest case of a multilayer grating structure. The synchronicity criteria that were derived for particle acceleration from these also applies to the multilayer grating structures described here. Without a loss in generality, in a typical configuration the incoming laser beam is at normal incidence with respect to the grating surface and its electric field is aligned with the grating grooves, corresponding to the TM polarization. The electron beam travels at a small elevation above a grating structure at a speed βc, where β is the speed normalized to the speed of light, and at an angle α, as shown in Figure 2. We shall define a coordinate system (x, y, z) for the electromagnetic field components that are aligned with the grating grooves, and another coordinate system (x', y', z') that is aligned with the particle's trajectory for the force components. The geometry can be viewed as a three-layer grating structure having a first vacuum layer $0 < y < +\infty$

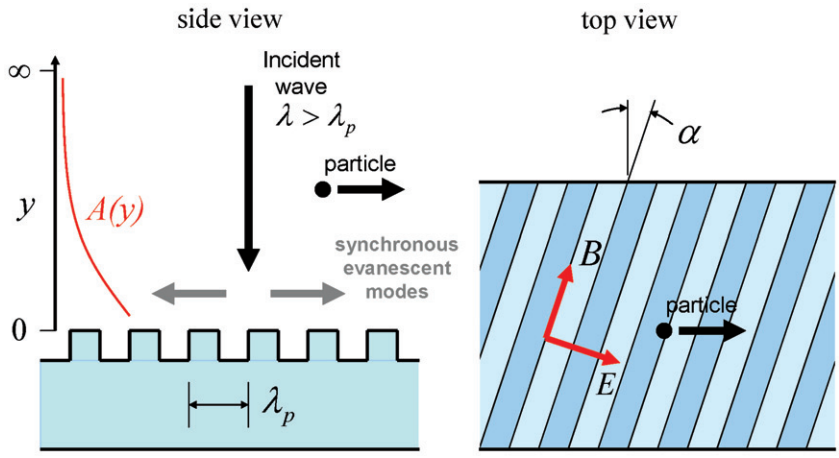

Figure 2. The open-grating geometry. The amplitude of the evanescent mode that interacts with the particle beam is an exponentially decaying function with elevation above the grating surface. (The color version of this figure is included in the online version of the journal.)

Downloaded by [Stanford University] at 16:19 16 August 2013

followed by a layer formed by the grating grooves and a last layer of uniform dielectric material. Within the vacuum layer the first grating diffraction mode is phase-synchronous with the particle when the wavelength λ and the grating period λ_p are related by

$$\lambda_p = \lambda\beta\cos\alpha. \tag{12}$$

Since $|\beta| < 1$ and $|\cos\alpha| \leq 1$ the grating grooves have a period smaller than the laser wavelength, that is, $\lambda_p < \lambda$. This phase-synchronous mode can be shown to correspond to first space harmonic having a positive eigenvalue for the matrix in Equation (3). It is therefore is evanescent and its strength decays exponentially with elevation above the grating structure at a rate

$$\Gamma = \sqrt{k_p^2 - k^2}. \tag{13}$$

Such a mode is highly asymmetric with elevation above the grating surface. A conventional particle beam travelling above the grating has a nonzero width in the y direction and is therefore distorted by this force pattern.

The non-uniform field pattern from the evanescent modes is a motivation to explore the effectiveness of the non-evanescent ones for particle manipulation. However, the non-evanescent modes propagate at the speed of light of the medium (in this case vacuum) and therefore their phase velocity projected on the particle beam can only be equal or larger than c [3]. The special case where the non-evanescent mode is synchronous with c occurs when $\alpha = 0$ and when $\lambda = \lambda_p$, which corresponds to a wave that satisfies Equation (6). Since the boundary of the vacuum layer above the grating is at $y \to \infty$ Equation (7) reveals that the mode amplitude must be zero.

6. Symmetric closed-channel grating structures

A layered grating structure of transparent material that contains a finite-width vacuum channel brings about two important advantages over open gratings. First, the vacuum channel can support a nonzero amplitude speed-of-light eigenmode that carries a longitudinal wave. Second, the multilayer structure can be symmetric and be driven from both sides by laser beams, as shown in Figure 3(*a*). The evanescent modes inside the vacuum channel produce a field pattern that due to symmetry has a hyperbolic cosine or hyperbolic sine profile. The structure is assumed to have the possibility of tilted grating grooves with respect to the particle beam direction just as the Smith Purcell structure in Figure 2. However, in contrast to the open gratings described before the structure is driven by two separate laser beams approaching the vacuum channel from opposite ends. These laser beams can be in or out of phase with respect to each other at the center of the vacuum channel, giving rise to a set of different focusing and steering force patterns that are analyzed in the next paragraphs.

Three possible structure configurations are described. The first is a structure that can support a speed-of-light longitudinal mode and therefore is meant for acceleration of relativistic particles. The second is a structure designed for acceleration of nonrelativistic particles, and the third is a deflector for relativistic and nonrelativistic particles. As mentioned before, because the eigenmode corresponding to the

Downloaded by [Stanford University] at 16:19 16 August 2013

first space harmonic is usually the largest, the structures described here have the grating period chosen such that the first harmonic in the vacuum channel is synchronous with the particle beam.

6.1. The speed-of-light mode, $\alpha = 0$ tilt structure

When the laser wavelength matches the grating period the modes presented in Equation (7) are one solution. This mode is relevant for particles travelling at speed of light in the x-direction. Two laser beams of equal amplitude applied to the grating from opposite sides generate a set of contributions whose magnetic field components can be described by

$$B_z^{(n,u)}(x,y,t) = \left(U_{-1}^{(n)}(1-\kappa y) + D_{-1}^{(n)}(1+\kappa y)\right)e^{ik_0 x - i\omega t + i\phi},$$
$$B_z^{(n,d)}(x,y,t) = \left(U_{-1}^{(n)}(1+\kappa y) + D_{-1}^{(n)}(1-\kappa y)\right)e^{ik_0 x - i\omega t + i\phi}, \tag{14}$$

where $B_z^{(n,u)}$ refers to magnetic field contribution from the upward propagating laser beam and $B_z^{(n,d)}$ to that from the downward propagating laser beam. The factor ϕ represents an overall phase between the input waves and the timing of the particle. The superscript letter n refers to the nth grating layer. When the relative phase of the electric field components of the input beams is equal at the center of the channel $y = 0$ the total field pattern is

$$E_x^{(n)}(x,y,t) = 2i\frac{c^2\kappa}{\omega}\left(D_{-1}^{(n)} - U_{-1}^{(n)}\right)e^{ik_0 x - i\omega t + i\phi},$$
$$E_y^{(n)}(x,y,t) = 2\kappa c y\left(D_{-1}^{(n)} - U_{-1}^{(n)}\right)e^{ik_0 x - i\omega t + i\phi},$$
$$B_z^{(n)}(x,y,t) = 2\kappa y\left(D_{-1}^{(n)} - U_{-1}^{(n)}\right)e^{ik_0 x - i\omega t + i\phi}. \tag{15}$$

The electromagnetic force on the charged particle beam is determined by Lorentz equation and is $\vec{F} = q\mathrm{Re}(\vec{E} + \vec{v} \times \vec{B})$. The mode in question is assumed to be synchronous with the particle. Therefore, the phases of the field components from the mode in question remain constant with respect to the particle and the resulting average force is equal to the instantaneous force. Here it is worth pointing out that the force from the non-synchronous modes oscillates with respect to the particle and therefore their extended contribution averages out. The Lorentz-force components from the fields in Equation (15) can be expressed as:

$$F_x^{(n)}(x,y,\phi) = -2q\frac{c^2\kappa}{\omega}\left(D_{-1}^{(n)} - U_{-1}^{(n)}\right)\sin\phi,$$
$$F_y^{(n)}(x,y,\phi) = 0,$$
$$F_z^{(n)}(x,y,\phi) = 0 \tag{16}$$

and are found to only contain an accelerating component. This force component is uniform across the entire vacuum channel, which is an important advantage over open grating accelerator structures since these can only accelerate particles with the non-uniform evanescent field pattern. Depending on the overall phase, which is captured by the term $\sin\phi$ in Equation (16), the force can be either accelerating or decelerating. In the notation employed here it is accelerating when $\phi = 3\pi/2$ (corresponding to $\sin\phi = -1$) and it is decelerating when $\phi = \pi/2$. When $\phi = 0$ the nominal force is zero, but note that for small positive deviations of phase it scales linearly with ϕ. With this condition of phase the mode generates a longitudinal focusing force pattern which is important for bunching of particle beams. In contrast, when the electric field components of the input waves are opposite the resulting force pattern is found to be $\vec{F}^{(n)}(x,y,t) = \vec{0}$, showing that this particular choice of phase configuration is not useful for manipulation of particles.

6.2. The slow-wave, $\alpha = 0$ tilt structure

In contrast to the previous case, for this condition the grating period is shorter than the laser wavelength and the first space harmonic in the vacuum channel is evanescent. To satisfy phase synchronicity of the first space harmonic inside the vacuum channel with a slow particle ($\beta < 1$) the grating k-vector must match the condition $\beta = k/k_p$. The magnetic field components of the first space harmonic in the vacuum channel produced by the up and the down input laser beams are described by the evanescent eigenmodes

$$B_z^{(n,u)}(x,y,t) = \left(U_{-1}^{(n)}e^{-\Gamma y} + D_{-1}^{(n)}\mathrm{e}^{+\Gamma y}\right)e^{ik_p x - i\omega t + i\phi},$$
$$B_z^{(n,d)}(x,y,t) = \left(U_{-1}^{(n)}\mathrm{e}^{+\Gamma y} + D_{-1}^{(n)}\mathrm{e}^{-\Gamma y}\right)\mathrm{e}^{ik_p x - i\omega t + i\phi}. \tag{17}$$

When the input wave electric field components are in-phase the resulting electromagnetic field pattern inside the vacuum channel is

$$E_x^{(n)}(x,y,t) = 2ic(\Gamma/k)\left(D_{-1}^{(n)} - U_{-1}^{(n)}\right)\cosh(\Gamma y)e^{ik_p x - i\omega t + i\phi},$$
$$E_y^{(n)}(x,y,t) = 2c(k_p/k)\left(D_{-1}^{(n)} - U_{-1}^{(n)}\right)\sinh(\Gamma y)e^{ik_p x - i\omega t + i\phi},$$
$$B_z^{(n)}(x,y,t) = 2\left(D_{-1}^{(n)} - U_{-1}^{(n)}\right)\sinh(\Gamma y)e^{ik_p x - i\omega t + i\phi}. \tag{18}$$

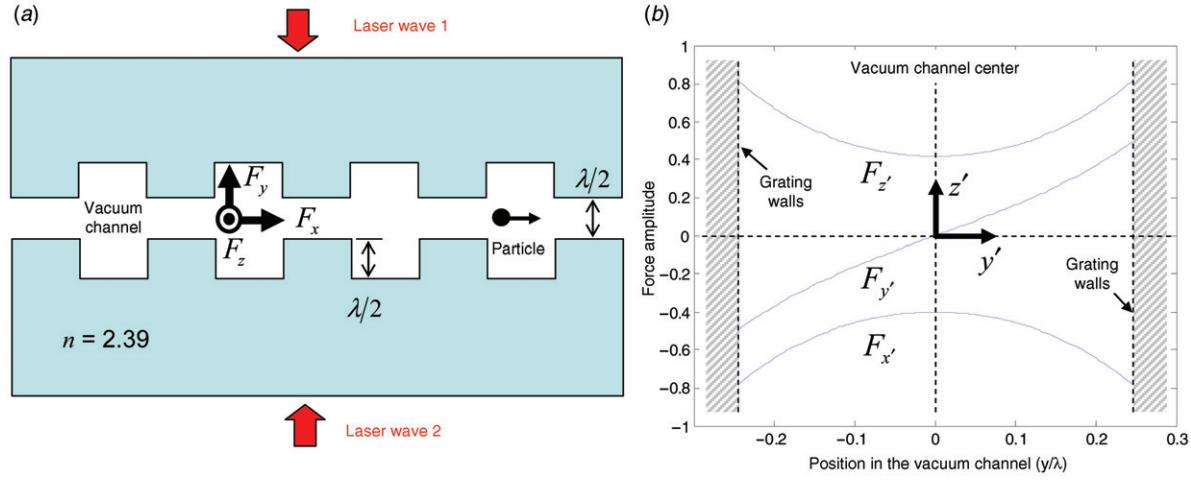

Figure 3. (*a*) Schematic of a possible symmetric binary grating structure powered by the laser beams from both sides. (*b*) Profile of the force components inside the vacuum channel on a particle traveling in a tilted grating structure. (The color version of this figure is included in the online version of the journal.)

Downloaded by [Stanford University] at 16:19 16 August 2013

The resulting Lorentz-force components are

$$F_x^{(n)}(x,y,t) = 2qc(\Gamma/k)\left(D_{-1}^{(n)} - U_{-1}^{(n)}\right)\cosh(\Gamma y)\sin\phi,$$
$$F_y^{(n)}(x,y,t) = 2q\left(D_{-1}^{(n)} - U_{-1}^{(n)}\right) \times \left(ck_p/k - v_x\right)\sinh(\Gamma y)\cos\phi,$$
$$F_z^{(n)}(x,y,t) = 0. \tag{19}$$

With this laser beam configuration the force pattern in the y-direction is a focusing force when $\phi = 0$ or defocusing force when $\phi = \pi$. When the particle is slipped by $\pi/2$ with respect to the laser beams the force pattern in the y-coordinate is turned off and a net acceleration force is generated. However, when the input wave electric field components are out-of-phase the resulting force components are

$$F_x^{(n)}(x,y,t) = -2qc(\Gamma/k)\left(U_{-1}^{(n)} + D_{-1}^{(n)}\right)\sinh(\Gamma y)\sin\phi,$$
$$F_y^{(n)}(x,y,t) = 2q\left(U_{-1}^{(n)} + D_{-1}^{(n)}\right)\left(ck_p/k - v_z\right) \times \cosh(\Gamma y)\cos\phi,$$
$$F_z^{(n)}(x,y,t) = 0. \tag{20}$$

Near the center of the vacuum channel ($y = 0$) and when $\phi = 0$ this configuration yields a nearly uniform deflection force directed towards one of the grating surfaces. The direction of the deflection force can be reversed by changing the phase of both laser beams by π. Note that the first correction factor with a spatial profile scales as $\Gamma^2 y^2$, so as long as the transverse beam dimension smaller than $1/(2\Gamma)$ the variation of the deflection force within the beam is about 3% of the magnitude on the center of the channel. To put this into perspective with the open grating structure, a shift in position by $1/(2\Gamma)$ results in 40% variation of the magnitude of the deflection force. Now, when the phase of the laser beams is changed by $\pi/2$ the deflection component vanishes and the acceleration component is maximized. Note, however, that this particular acceleration force pattern is not a desirable one since its biggest effect is to introduce energy spread to the particle beam rather than cause a net energy change.

6.3. *The $\alpha \neq 0$ tilt structure*

In this particular case the particle is traveling at an oblique orientation with respect to the grating grooves, as illustrated in Figure 2. In the grating's coordinates the particle's velocity is described by a vector of the form

$$\vec{v} = \beta c \begin{pmatrix} \cos\alpha \\ 0 \\ \sin\alpha \end{pmatrix}. \tag{21}$$

Again, assume phase synchronicity with the first space harmonic. Therefore the grating's k-vector satisfies $\beta\cos\alpha = k/k_p$, which means that the grating period is shorter than the laser wavelength and therefore the synchronous mode is evanescent. When the incident wave electric fields are in phase the field components are given by Equation (18). The resulting force pattern in the particle's coordinate system is given by

$$F_{x'}^{(n)}(x,y,t) = -2qc(\Gamma/k)\left(D_{-1}^{(n)} - U_{-1}^{(n)}\right) \times \cosh(\Gamma y)\sin\phi\cos\alpha,$$
$$F_{y'}^{(n)}(x,y,t) = 2qc\left(D_{-1}^{(n)} - U_{-1}^{(n)}\right)\sinh(\Gamma y) \times (1/(\beta\cos\alpha) - \beta\cos\alpha)\cos\phi,$$

Downloaded by [Stanford University] at 16:19 16 August 2013

Table 1. Force pattern dependence on grating geometry, laser phase and velocity.

		Grating tilt angle $\alpha = 0$				Grating tilt angle $\alpha \neq 0$			
		Laser beams in phase		Laser beams out of phase		Laser beams in phase		Laser beams out of phase	
	β	$\phi = 0$	$\phi = \pi/2$	$\phi = 0$	$\phi = \pi/2$	$\phi = 0$	$\phi = \pi/2$	$\phi = 0$	$\phi = \pi/2$
TM	1	0	0	0	Acceleration	Deflection y-axis	Skew acceleration pattern	Focusing y-axis	Deflection z-axis and acceleration
	<1	Deflection y-axis	Skew acceleration pattern	Focusing y-axis	Acceleration	Deflection y-axis	Skew acceleration pattern	Focusing y-axis	Deflection z-axis and acceleration
TE	1	0	0	0	0	Deflection z-axis and acceleration	Focusing y-axis	Skew acceleration pattern	Deflection y-axis
	<1	0	0	0	0	Deflection z-axis and acceleration	Focusing y-axis	Skew acceleration pattern	Deflection y-axis

$$F_{z'}^{(n)}(x,y,t) = 2qc(\Gamma/k)\left(D_{-1}^{(n)} - U_{-1}^{(n)}\right) \times \cosh(\Gamma y)\sin\phi\sin\alpha. \quad (22)$$

The force pattern is either a focusing force pattern in the y-coordinate when $\phi = 0$ and a deflection force parallel to the grating (in the z-coordinate) walls that is accompanied by a uniform acceleration component when $\phi = \pi/2$. If needed, the acceleration component can be selectively cancelled out by adding a second grating section of equal length with a laser phase $\phi = -\pi/2$. Figure 3(*b*) shows an example for the force pattern from a 40° tilted grating structure with the dimensions shown in Figure 3(*a*) and for the conditions in Equation (22) acting on relativistic charged particles. When the incident wave electric fields have opposite phase the force components expressed in the particle's coordinates are

$$\begin{aligned} F_{x'}^{(n)}(x,y,t) &= -2qc(\Gamma/k)\left(U_{-1}^{(n)} + D_{-1}^{(n)}\right) \times \sinh(\Gamma y)\sin\phi\cos\alpha, \\ F_{y'}^{(n)}(x,y,t) &= 2qc\left(U_{-1}^{(n)} + D_{-1}^{(n)}\right)\cosh(\Gamma y) \times (1/(\beta\cos\alpha) + \beta\cos\alpha)\cos\phi, \\ F_{z'}^{(n)}(x,y,t) &= 2qc(\Gamma/k)\left(U_{-1}^{(n)} + D_{-1}^{(n)}\right) \times \sinh(\Gamma y)\sin\phi\sin\alpha. \end{aligned} \quad (23)$$

When the optical phase $\phi = 0$ the effective pattern generates a nearly uniform deflection in the y-coordinate, which is a useful configuration. However, when shifted by $\pi/2$ the resulting force provides a skewed acceleration pattern that introduces energy spread to the beam.

6.4. The TE polarization

For the TE polarization the electric field is aligned with the grating grooves and the magnetic field lies in the *xy* plane. The same kind of analysis shows that for this polarization the $\alpha = 0$ tilt structure is unable to generate an acceleration force regardless of the laser phase or particle velocity. For the $\alpha \neq 0$ tilt structure it is found that similar to the TM polarization a deflection, acceleration and focusing force pattern is also possible to be generated. Table 1 summarizes the resulting force patterns from the possible laser phase, polarization and grating tilt angle condition. The $\alpha = 0$ grating geometry shows a clear advantage of the TM over the TE polarization in the ability to generate a uniform acceleration force.

In summary, the same multilayer binary grating accelerator structure can generate acceleration, deflection or focusing forces on a charged particle beam by adjustment of the phase and polarization of the incident laser beams. Furthermore, closed symmetric grating structures show a clear advantage over open grating structures both in their ability to support speed-of-light longitudinal waves for uniform acceleration and for generating a symmetric force pattern.

7. Outlook

This paper demonstrates the general applicability of simple closed channel grating structures for their use as ultrafast particle beam manipulation elements. Stacking of these elements is envisioned as a means for providing an extended charged particle beam transport system that is entirely based on laser-driven photonic structures. Upcoming work will focus on a higher-order analysis of some of the force patterns described here. For instance, while the TE polarization does not generate an accelerating or a deflection force on the design-orbit particle (traveling at the center of the vacuum channel and with no transverse velocity component) it does provide a solenoid field (a magnetic field component aligned with the particle's direction of motion) whose focusing properties merit closer attention. Furthermore, closer inspection of Table 1 reveals that spatial focusing is only provided in the *y*-axis. This is due to the assumed translational invariance along the grating groove. A closer inspection of the effect of a finite sized laser beam or a curved grating groove is expected to reveal the existence of spatial focusing in the other spatial coordinate. Finally, an in-depth analysis of the aberrations from these photonic structure elements and their impact on beam emittance will determine the feasibility of multilayer gratings as elements of an extended beam transport system.

References

[1] Pickup, M.A. A Linear Accelerator Using Gratings. Ph.D. Thesis, Cornell University, 1987.

[2] Plettner, T.; Lu, P.P.; Byer, R.L. *Phys. Rev. Spec. Top.–Accel. Beams* **2006,** *9,* 111301.

[3] Palmer, R. *Open Accelerating Structures;* SLAC-PUB-4161, 1986.

[4] Cowan, B.M. *Phys. Rev. Spec. Top.–Accel. Beams* **2003,** *6,* 101301.

[5] Cowan, B.M. *Phys. Rev. Spec. Top.–Accel. Beams* **2008,** *11,* 011301.

[6] Rosenzweig, J.; Murokh, A.; Pellegrini, C. *Phys. Rev. Lett.* **1995,** *74,* 002467.

[7] Plettner, T.; Byer, R.L.; McGuinness, C.; Hommelhoff, P. *Phys. Rev. Spec. Top.–Accel. Beams* **2009,** *12,* 101302.

[8] Pai, D.M.; Awada, K.A. *J. Opt. Soc. Am. A* **1991,** *8,* 755–762.

Downloaded by [Stanford University] at 16:19 16 August 2013

[9] Wangler, T. *Principles of RF Linear Accelerators*; Wiley Interscience: New York, 1998; pp 58–62.
[10] Mizuno, K.; Pae, J.; Nozodiko, T.; Furuya, K. *Nature* **1987,** *328,* 45–47.
[11] Bae, J.; Furuya, K.; Shirai, H.; Nozokido, T.; Mizuno, K. *Jpn. J. Appl. Phys.* **1988,** *27,* 408–412.
[12] Smith, S.J.; Purcell, E.M. *Phys. Rev.* **1953,** *92,* 1069–1069.
[13] Korbly, S.E.; Kesar, A.S.; Sirigiri, J.R.; Temkin, R.J. *Phys. Rev. Lett.* **2005,** *94,* 054803.
[14] Magnusson, R.; Shin, D.; Liu, Z.S. *Opt. Lett.* **1998,** *23,* 612–614.

Downloaded by [Stanford University] at 16:19 16 August 2013

Appendix 1. Derivation of the transmission and reflection coefficients

This section derives the values of the interface transmission and reflection coefficients between adjacent grating layers. An upward propagating wave emerging above a layer interface has to satisfy the boundary condition with the upward and downward waves below the interface. This sets a condition for the interface matrices that reads

$$\begin{pmatrix} \mathbf{u}_+^{(n)} \\ \mathbf{d}_+^{(n)} \end{pmatrix} = \begin{pmatrix} \mathbf{C}_{uu}^{(n)} & \mathbf{C}_{ud}^{(n)} \\ \mathbf{C}_{du}^{(n)} & \mathbf{C}_{dd}^{(n)} \end{pmatrix} \begin{pmatrix} \mathbf{u}_-^{(n+1)} \\ 0 \end{pmatrix}. \tag{24}$$

An analogous situation is true for the downward propagating wave emerging below a layer interface.

$$\begin{pmatrix} 0 \\ \mathbf{d}_+^{(n)} \end{pmatrix} = \begin{pmatrix} \mathbf{C}_{uu}^{(n)} & \mathbf{C}_{ud}^{(n)} \\ \mathbf{C}_{du}^{(n)} & \mathbf{C}_{dd}^{(n)} \end{pmatrix} \begin{pmatrix} \mathbf{u}_-^{(n+1)} \\ \mathbf{d}_-^{(n+1)} \end{pmatrix}. \tag{25}$$

The iterative approach applies the boundary conditions to one pair of modes at a time. For example the jth up mode above the boundary is related to the sum of up and down modes below the boundary

$$\begin{aligned} &\mathbf{V}_j^{(n+1)} u_j^{(n+1)}\left(y_-^{(n+1)}\right) = \sum_{l=-N}^{N} \mathbf{V}_l^{(n)} \left(u_l^{(n)}\left(y_+^{(n)}\right) + d_l^{(n)}\left(y_+^{(n)}\right)\right) \\ &\mathbf{S}^{(n)}\left(\mathbf{S}^{(n+1)}\right)^{-1} \mathbf{V}_j^{(n+1)} d_y u_j^{(n+1)}\left(y_-^{(n+1)}\right) \\ &\quad = \sum_{l=-N}^{N} \mathbf{V}_l^{(n)} d_y \left(u_l^{(n)}\left(y_+^{(n)}\right) + d_l^{(n)}\left(y_+^{(n)}\right)\right), \end{aligned} \tag{26}$$

where $\mathbf{V}_j^{(n)}$ is the jth eigenvector that matches the jth eigenvalue of matrix $\mathbf{K}+\mathbf{S}^{(n)}$ in layer n. There are four possible cases for the up mode solution of the nth layer depending on whether the eigenvalue of the eigenmodes in question are zero or nonzero. The original formulation only describes the first case with nonzero eigenvalues above and below the interface, when in fact there is a total of four possible cases that will be described next. Denote the nonzero eigenvalue of the jth upper layer mode $e_j^{(n+1)}$ and the ith lower layer mode $e_i^{(n)}$. Multiplication on both sides of the boundary conditions in Equation (26) by $\left(\mathbf{V}_i^{(n)}\right)^\dagger$ allows for their diagonalization, and to evaluate a pair of the matrix coupling coefficients of Equations (24) and (25).

A1.1. Upper and lower layer eigenvalues are nonzero

$$\begin{aligned} &\left(\mathbf{C}_{uu}\right)_{ij}^{(n)} \\ &\quad \equiv \frac{u_i^{(n)}\left(y_+^{(n)}\right)}{u_j^{(n+1)}\left(y_-^{(n+1)}\right)} \\ &\quad = \frac{e_i^{(n)}\left(\left(\mathbf{V}_i^{(n)}\right)^\dagger \cdot \mathbf{V}_j^{(n+1)}\right) + e_j^{(n+1)}\left(\left(\mathbf{V}_i^{(n)}\right)^\dagger \cdot \mathbf{S}^{(n)}\left(\mathbf{S}^{(n+1)}\right)^{-1} \cdot \mathbf{V}_j^{(n+1)}\right)}{2e_i^{(n)}} \\ &\left(\mathbf{C}_{du}\right)_{ij}^{(n)} \\ &\quad \equiv \frac{d_i^{(n)}\left(y_+^{(n)}\right)}{u_j^{(n+1)}\left(y_-^{(n+1)}\right)} \\ &\quad = \frac{e_i^{(n)}\left(\left(\mathbf{V}_i^{(n)}\right)^\dagger \cdot \mathbf{V}_j^{(n+1)}\right) - e_j^{(n+1)}\left(\left(\mathbf{V}_i^{(n)}\right)^\dagger \cdot \mathbf{S}^{(n)}\left(\mathbf{S}^{(n+1)}\right)^{-1} \cdot \mathbf{V}_j^{(n+1)}\right)}{2e_i^{(n)}}. \end{aligned} \tag{27a}$$

A2.1. Upper layer eigenvalue is zero

$$\begin{aligned} \left(\mathbf{C}_{uu}\right)_{ij}^{(n)} &\equiv \frac{u_i^{(n)}\left(y_+^{(n)}\right)}{U_j^{(n+1)}} \\ &= \frac{\left\{ \begin{array}{l} ie_i^{(n)}\left(\left(\mathbf{V}_i^{(n)}\right)^\dagger \cdot \mathbf{V}_j^{(n+1)}\right)\left(1-\kappa^{(n+1)} y_-^{(n+1)}\right) \\ \quad -\kappa^{(n+1)}\left(\left(\mathbf{V}_i^{(n)}\right)^\dagger \cdot \mathbf{S}^{(n)}\left(\mathbf{S}^{(n+1)}\right)^{-1} \cdot \mathbf{V}_j^{(n+1)}\right) \end{array} \right\}}{2ie_i^{(n)}} \\ \left(\mathbf{C}_{du}\right)_{ij}^{(n)} &\equiv \frac{u_i^{(n)}\left(y_+^{(n)}\right)}{U_j^{(n+1)}} \\ &= \frac{\left\{ \begin{array}{l} ie_i^{(n)}\left(\left(\mathbf{V}_i^{(n)}\right)^\dagger \cdot \mathbf{V}_j^{(n+1)}\right)\left(1-\kappa^{(n+1)} y_-^{(n+1)}\right) \\ \quad +\kappa^{(n+1)}\left(\left(\mathbf{V}_i^{(n)}\right)^\dagger \cdot \mathbf{S}^{(n)}\left(\mathbf{S}^{(n+1)}\right)^{-1} \cdot \mathbf{V}_j^{(n+1)}\right) \end{array} \right\}}{2ie_i^{(n)}}. \end{aligned} \tag{27b}$$

A3.1. Lower layer eigenvalue is zero

$$\begin{aligned} \left(\mathbf{C}_{uu}\right)_{ij}^{(n)} &\equiv \frac{U_i^{(n)}}{u_j^{(n+1)}\left(y_-^{(n+1)}\right)} \\ &= \frac{\kappa^{(n)}\left\{ \begin{array}{l} \left(\left(\mathbf{V}_i^{(n)}\right)^\dagger \cdot \mathbf{V}_j^{(n+1)}\right) - ie_j^{(n+1)}\left(1-\kappa^{(n)} y_+^{(n)}\right) \\ \quad \times \left(\left(\mathbf{V}_i^{(n)}\right)^\dagger \cdot \mathbf{S}^{(n)}\left(\mathbf{S}^{(n+1)}\right)^{-1} \cdot \mathbf{V}_j^{(n+1)}\right) \end{array} \right\}}{2\kappa^{(n)}} \\ \left(\mathbf{C}_{du}\right)_{ij}^{(n)} &\equiv \frac{D_i^{(n)}}{u_j^{(n+1)}\left(y_-^{(n+1)}\right)} \end{aligned}$$

$$= \frac{\kappa^{(n)}\left\{\begin{array}{l}\left(\left(\mathbf{V}_i^{(n)}\right)^{\dagger}\cdot\mathbf{V}_j^{(n+1)}\right)+ie_j^{(n+1)}\left(1+\kappa^{(n)}y_+^{(n)}\right)\\ \quad\times\left(\left(\mathbf{V}_i^{(n)}\right)^{\dagger}\cdot\mathbf{S}^{(n)}\left(\mathbf{S}^{(n+1)}\right)^{-1}\cdot\mathbf{V}_j^{(n+1)}\right)\end{array}\right\}}{2\kappa^{(n)}}. \quad (27c)$$

A4.1. Eigenvalues on both layers are zero

$$(\mathbf{C}_{uu})_{ij}^{(n)} \equiv \frac{U_i^{(n)}}{U_j^{(n+1)}} = \frac{\left\{\begin{array}{l}\left(1-\kappa^{(n+1)}y_-^{(n+1)}\right)\kappa^{(n)}\left(\left(\mathbf{V}_i^{(n)}\right)^{\dagger}\cdot\mathbf{V}_j^{(n+1)}\right)+\kappa^{(n+1)}\\ \quad\times\left(1+\kappa^{(n)}y_+^{(n)}\right)\left(\left(\mathbf{V}_i^{(n)}\right)^{\dagger}\cdot\mathbf{S}^{(n)}\left(\mathbf{S}^{(n+1)}\right)^{-1}\cdot\mathbf{V}_j^{(n+1)}\right)\end{array}\right\}}{2\kappa^{(n)}}$$

$$(\mathbf{C}_{du})_{ij}^{(n)} \equiv \frac{D_i^{(n)}}{U_j^{(n+1)}} = \frac{\left\{\begin{array}{l}\left(1-\kappa^{(n+1)}y_-^{(n+1)}\right)\kappa^{(n)}\left(\left(\mathbf{V}_i^{(n)}\right)^{\dagger}\cdot\mathbf{V}_j^{(n+1)}\right)-\kappa^{(n+1)}\\ \quad\times\left(1-\kappa^{(n)}y_+^{(n)}\right)\left(\left(\mathbf{V}_i^{(n)}\right)^{\dagger}\cdot\mathbf{S}^{(n)}\left(\mathbf{S}^{(n+1)}\right)^{-1}\cdot\mathbf{V}_j^{(n+1)}\right)\end{array}\right\}}{2\kappa^{(n)}}. \quad (27d)$$

The analysis for the down-propagating wave proceeds in a similar fashion. The up- and down propagating modes above the interface are evaluated as a function of the down-propagating mode below the layer interface, which allows to determine an equivalent pair of coupling coefficients.

A5.1. Upper and lower layer eigenvalues are nonzero

$$\mathbf{W}_{ij}^{(n)} \equiv \frac{u_i^{(n+1)}\left(y_-^{(n+1)}\right)}{d_j^{(n)}\left(y_+^{(n)}\right)} = \frac{\left\{\begin{array}{l}e_i^{(n+1)}\left(\left(\mathbf{V}_i^{(n+1)}\right)^{\dagger}\cdot\mathbf{V}_j^{(n)}\right)\\ \quad-e_j^{(n)}\left(\left(\mathbf{V}_i^{(n+1)}\right)^{\dagger}\cdot\mathbf{S}^{(n+1)}\left(\mathbf{S}^{(n)}\right)^{-1}\cdot\mathbf{V}_j^{(n)}\right)\end{array}\right\}}{2e_i^{(n+1)}}$$

$$\mathbf{H}_{ij}^{(n)} \equiv \frac{d_i^{(n+1)}\left(y_-^{(n+1)}\right)}{d_j^{(n)}\left(y_+^{(n)}\right)} = \frac{\left\{\begin{array}{l}e_i^{(n+1)}\left(\left(\mathbf{V}_i^{(n+1)}\right)^{\dagger}\cdot\mathbf{V}_j^{(n)}\right)\\ \quad+e_j^{(n)}\left(\left(\mathbf{V}_i^{(n+1)}\right)^{\dagger}\cdot\mathbf{S}^{(n+1)}\left(\mathbf{S}^{(n)}\right)^{-1}\cdot\mathbf{V}_j^{(n)}\right)\end{array}\right\}}{2e_i^{(n+1)}}. \quad (28a)$$

A6.1. Upper layer eigenvalue is zero

$$\mathbf{W}_{ij}^{(n)} \equiv \frac{U_i^{(n+1)}}{d_j^{(n)}\left(y_+^{(n)}\right)} = \frac{\left\{\begin{array}{l}\left(\left(\mathbf{V}_i^{(n+1)}\right)^{\dagger}\cdot\mathbf{V}_j^{(n)}\right)\kappa\mathbf{R}_{du}^{(n)}(n+1)+ie_j^{(n)}\left(1+\kappa^{(n+1)}y_-^{(n+1)}\right)\\ \quad\times\left(\left(\mathbf{V}_i^{(n+1)}\right)^{\dagger}\cdot\mathbf{S}^{(n+1)}\left(\mathbf{S}^{(n)}\right)^{-1}\cdot\mathbf{V}_j^{(n)}\right)\end{array}\right\}}{2\kappa^{(n+1)}}$$

$$\mathbf{H}_{ij}^{(n)} \equiv \frac{D_i^{(n+1)}}{d_j^{(n)}\left(y_+^{(n)}\right)} = \frac{\left\{\begin{array}{l}\left(\left(\mathbf{V}_i^{(n+1)}\right)^{\dagger}\cdot\mathbf{V}_j^{(n)}\right)\kappa^{(n+1)}-ie_j^{(n)}\left(1-\kappa^{(n+1)}y_-^{(n+1)}\right)\\ \quad\times\left(\left(\mathbf{V}_i^{(n+1)}\right)^{\dagger}\cdot\mathbf{S}^{(n+1)}\left(\mathbf{S}^{(n)}\right)^{-1}\cdot\mathbf{V}_j^{(n)}\right)\end{array}\right\}}{2\kappa^{(n+1)}}. \quad (28b)$$

A7.1. Lower layer eigenvalue is zero

$$\mathbf{W}_{ij}^{(n)} \equiv \frac{u_i^{(n+1)}\left(y_-^{(n+1)}\right)}{D_j^{(n)}} = \frac{\left\{\begin{array}{l}ie_i^{(n+1)}\left(\left(\mathbf{V}_i^{(n+1)}\right)^{\dagger}\cdot\mathbf{V}_j^{(n)}\right)\left(1+\kappa^{(n)}y_+^{(n)}\right)\\ \quad+\kappa^{(n)}\left(\left(\mathbf{V}_i^{(n+1)}\right)^{\dagger}\cdot\mathbf{S}^{(n+1)}\left(\mathbf{S}^{(n)}\right)^{-1}\cdot\mathbf{V}_j^{(n)}\right)\end{array}\right\}}{2ie_i^{(n+1)}}$$

$$\mathbf{H}_{ij}^{(n)} \equiv \frac{d_i^{(n+1)}\left(y_-^{(n+1)}\right)}{D_j^{(n)}} = \frac{\left\{\begin{array}{l}ie_i^{(n+1)}\left(\left(\mathbf{V}_i^{(n+1)}\right)^{\dagger}\cdot\mathbf{V}_j^{(n)}\right)\left(1+\kappa^{(n)}y_+^{(n)}\right)\\ \quad-\kappa^{(n)}\left(\left(\mathbf{V}_i^{(n+1)}\right)^{\dagger}\cdot\mathbf{S}^{(n+1)}\left(\mathbf{S}^{(n)}\right)^{-1}\cdot\mathbf{V}_j^{(n)}\right)\end{array}\right\}}{2ie_i^{(n+1)}}. \quad (28c)$$

A8.1. Eigenvalues on both layers are zero

$$\mathbf{W}_{ij}^{(n)} \equiv \frac{U_i^{(n+1)}}{D_j^{(n)}} = \frac{\left\{\begin{array}{l}\left(\left(\mathbf{V}_i^{(n+1)}\right)^{\dagger}\cdot\mathbf{V}_j^{(n)}\right)\left(1+\kappa^{(n)}y_+^{(n)}\right)\kappa^{(n+1)}\\ \quad-\left(\left(\mathbf{V}_i^{(n+1)}\right)^{\dagger}\cdot\mathbf{S}^{(n+1)}\left(\mathbf{S}^{(n)}\right)^{-1}\cdot\mathbf{V}_j^{(n)}\right)\left(1+\kappa^{(n+1)}y_-^{(n+1)}\right)\end{array}\right\}}{2\kappa^{(n+1)}}$$

$$\mathbf{H}_{ij}^{(n)} \equiv \frac{D_i^{(n+1)}}{D_j^{(n)}}$$

Downloaded by [Stanford University] at 16:19 16 August 2013

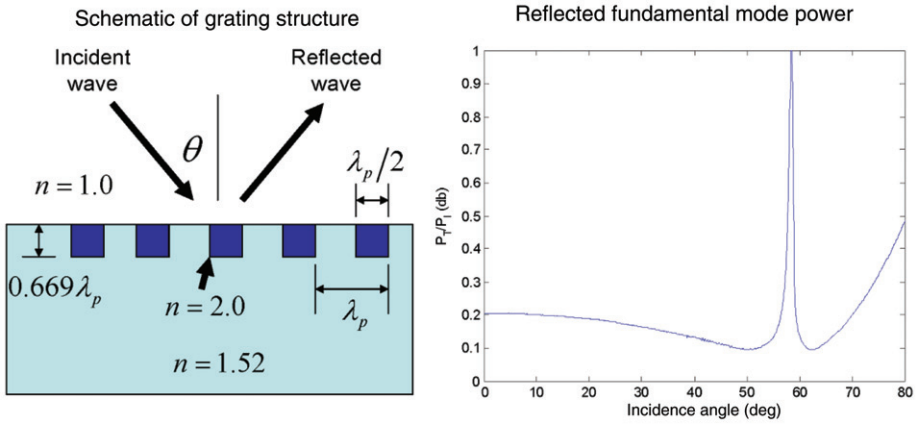

Figure 4. Map of the photonic grating structure and the reflectance as a function of incidence angle. The grating period λ_p is 266.2 nm and the incident laser wavelength λ is 632.8 nm. The polarization of the incident wave is TM. (The color version of this figure is included in the online version of the journal.)

$$= \frac{\left\{ \begin{array}{l} \left(\left(\mathbf{V}_i^{(n+1)} \right)^{\dagger} \cdot \mathbf{V}_j^{(n)} \right) \left(1 + \kappa^{(n)} y_+^{(n)} \right) \kappa^{(n+1)} \\ \quad + \left(\left(\mathbf{V}_i^{(n+1)} \right)^{\dagger} \cdot \mathbf{S}^{(n+1)} \left(\mathbf{S}^{(n)} \right)^{-1} \cdot \mathbf{V}_j^{(n)} \right) \left(1 - \kappa^{(n+1)} y_-^{(n+1)} \right) \end{array} \right\}}{2\kappa^{(n+1)}} \tag{28d}$$

where the matrices $\mathbf{W}^{(n)}$ and $\mathbf{H}^{(n)}$ are related to the coupling coefficients of Equations (24) and (25) by

$$\begin{aligned} \mathbf{C}_{dd}^{(n)} &= \left(\mathbf{I} - \mathbf{C}_{du}^{(n)} \mathbf{W}^{(n)} \mathbf{H}^{(n)} \right) \left(\mathbf{H}^{(n)} \right)^{-1}, \\ \mathbf{C}_{ud}^{(n)} &= -\mathbf{C}_{uu}^{(n)} \mathbf{W}^{(n)} \left(\mathbf{H}^{(n)} \right)^{-1}. \end{aligned} \tag{29}$$

In the same manner as derived by Pai and Awada the specific mode reflection and transmission matrices can be defined in terms of the coupling matrices by

$$\begin{aligned} \mathbf{R}_{ud}^{(n)} &= -\left(\mathbf{C}_{uu}^{(n)} \right)^{-1} \mathbf{C}_{ud}^{(n)}, \\ \mathbf{T}_{dd}^{(n)} &= \mathbf{C}_{dd}^{(n)} - \mathbf{C}_{du}^{(n)} \left(\mathbf{C}_{uu}^{(n)} \right)^{-1} \mathbf{C}_{ud}^{(n)}, \\ \mathbf{T}_{uu}^{(n)} &= \left(\mathbf{C}_{uu}^{(n)} \right)^{-1}, \\ \mathbf{R}_{du}^{(n)} &= \mathbf{C}_{du}^{(n)} \left(\mathbf{C}_{uu}^{(n)} \right)^{-1}. \end{aligned} \tag{30}$$

The numerical solution is based on propagating an input wave through the grating layers, and then propagating the reflections from each layer interface toward the other direction. This iteration of successively propagating the reflected waves from each layer interface is repeated several times until the contribution to the total wave becomes negligible. The total wave is the sum of the initial wave plus the reflected up and down waves calculated from the iterative approach.

The eigenmode decomposition method is tested with an example of a guided mode resonance Brewster filter that acts as a high reflector mirror for TM polarized waves of a particular wavelength at Brewster incidence [14]. The photonic device is a grating structure whose cross-section is shown in Figure 4. Here the same structure geometry is analyzed with the multilayer grating decomposition method. The geometry can be broken down into three layers; one very thick ($10^6\lambda$) air layer, the middle layer containing the index modulation, and a third thick layer describing the bulk index material. The curve for reflectance as a function of incidence angle θ is computed as the ratio between the power of the downward and the upward modes corresponding to the zero-order space harmonics in the air layer. It shows a sharp reflectance peak that is in close agreement with the reference.

Downloaded by [Stanford University] at 16:19 16 August 2013